Chem. Erde **54** (1994), 297–318
Gustav Fischer Verlag Jena

Petrographical and Geochronological Investigations on a Garnet-Tourmaline Pegmatite from Ringgold Knoll, Oates Coast, Antarctica*

Petrographische und geochronologische Untersuchungen an einem Granat-Turmalin-Pegmatit vom Ringgold Knoll, Oates Coast, Antarktis

ULRICH SCHÜSSLER and FRIEDHELM HENJES-KUNST

Mineralogical Institute, University Würzburg, Germany
Federal Institute for Geosciences and Natural Resources, Hannover, Germany

With 8 Figures

(Received 28. July 1994; accepted in revised form 3. August 1994)

Abstract

The Ringgold Knoll pegmatite, a late-stage member of the Granite Harbour Intrusives, crosscuts high-grade Wilson gneisses of the Oates Coast, which forms the westernmost part of the Wilson Terrane at the Pacific end of the Cambro-Ordovician Ross orogenic belt in West Antarctica. The pegmatite mineral assemblage consists of K-feldspar, plagioclase, quartz, garnet (almandine-spessartine-pyrope), dark tourmaline (schorl-dravite), muscovite, apatite, monazite, zircon, blue Al-rich tourmaline and dumortierite in order of decreasing abundances. Major, minor and rare earth elements are reported for the greater part of the mineral assemblage. The time of pegmatite emplacement is constrained by Rb-Sr and Sm-Nd isochron ages of 492 ± 8 (2σ) Ma and 500 ± 40 (2σ) Ma, respectively. High initial $^{87}Sr/^{86}Sr$ of 0.7315 ± 0.0003 and low ϵ Nd,t of –8.7 ± 1.2 strongly support an origin of the magma from highly evolved crustal source rocks. K-Ar and ^{40}Ar-^{39}Ar model ages of about 470 to 475 Ma for igneous muscovite indicate that the pegmatite together with its wall rocks spent a prolonged period at elevated temperatures before final cooling below about 350 °C. The muscovite dates may give an estimate for the time of exhumation of the Oates Coast crystalline basement along two major late Ross orogenic detachment zones within the Wilson Terrane i.e. the Wilson and the Exiles thrusts (c.f. FLÖTTMANN and KLEINSCHMIDT, 1991).

Zusammenfassung

Der Pegmatit vom Ringgold Knoll gehört zur späten Gangfolge der Granite Harbour Intrusionen und durchschlägt hochgradig metamorphe Wilson Gneise der Oates Coast, die den westlichsten Teil des Wilson Terranes am pazifischen Ende des Kambro-Ordovizischen Ross Orogengürtels in

* Dedicated to Professor Dr. MARTIN OKRUSCH on the occasion of his 60th birthday.

der Westantarktis bildet. Die pegmatitische Mineralparagenese besteht aus Kalifeldspat, Plagioklas, Quarz, almandin-spessartin-pyrop-betontem Granat, dunklem schörl-dravit-betontem Turmalin, Muscovit, Apatit, Monazit, Zirkon, blauem Al-reichem Turmalin und Dumortierit in der Reihenfolge abnehmenden Modalanteils. Für den größeren Teil der Minerale wurden Haupt-, Neben- und Seltenerdelemente bestimmt. Der Zeitpunkt der Pegmatitintrusion wird durch Rb-Sr und Sm-Nd Isochronenalter von 492 ± 8 (2σ) Ma bzw. 500 ± 40 Ma (2σ) datiert. Ein hohes $^{87}Sr/^{86}Sr$ Initialverhältnis von 0,7315 ± 0,0003 und ein niedriger Wert für ϵ Nd,t von –8,7 ± 1,2 sprechen deutlich für eine Magmenherkunft von hochdifferenzierten krustalen Ausgangsgesteinen. K-Ar und ^{40}Ar-^{39}Ar Modellalter von etwa 470 bis 475 Ma von magmatischem Muscovit zeigen, daß der Pegmatit und das Nebengestein eine langsame Abkühlung auf Temperaturen unter etwa 350 °C erlebten. Die Muscovitdaten können als eine Zeitmarke gesehen werden für die Heraushebung des kristallinen Grundgebirges der Oates Coast entlang der zwei spät Ross-orogenen Wilson und Exiles Hauptüberschiebungszonen im Wilson Terrane (FLÖTTMANN und KLEINSCHMIDT 1991).

Introduction

The Oates Coast and the easternly adjoining North Victoria Land form the Pacific end of the Transantarctic Mountains, Antarctica. The Oates Coast was visited during the German Antarctic North Victoria Land Expeditions GANOVEX V and VII, carried out in 1988/89 and 1992/93 by the German Federal Institute for Geosciences and Natural Resources (BGR). Large-scale geological mapping of this area was performed for the first time (GANOVEX-TEAM, in prep.). At the westernmost summit ridge of Ringgold Knoll, located east of the Matusevich glacier (Fig. 1), a pegmatite with conspicuous, partly graphophyric intergrowths of quartz and tourmaline within a matrix of feldspar, quartz and garnet was discovered and sampled.

The Ringgold Knoll garnet-tourmaline pegmatite which forms part of the Cambrian to early Ordovician Granite Harbour Intrusives (GHI; GUNN and WARREN, 1962) is about two metres in thickness and shows no macroscopic signs of deformation. It crosscuts high-grade Wilson metamorphics, which at Ringgold Knoll are dominated by garnet-biotite gneisses with intercalations of calc-silicate layers and boudins of some centimetres to decimetres in thickness. Whereas plutonic members of the GHI have been the subject of abundant studies, the associated late-stage dyke rocks (i.e. aplites, pegmatites and fine-grained dykes) have only been rarely investigated. Because of the conspicuous mineral assemblage the Ringgold Knoll pegmatite calls for a detailed study of mineralogy and mineral chemistry, including major, minor and rare-earth element compositions.

Furthermore, the late-stage pegmatite may be regarded as a time marker for the waning tectono-magmatic evolution of the Cambro-Ordovician Ross Orogeny in the Oates Coast area. By applying different methods, radiometric dating of the minerals and whole-rock should allow the time of pegmatite emplacement to be constrained as well as its subsequent cooling history. In addition to the minerals normally used for age determinations, the complex mineral assemblage invites to test the reliability of minerals like tourmaline, monazite and apatite among others, for both Rb-Sr and Sm-Nd dating techniques.

Geological Setting

Basement rocks of the Oates Coast area form part of the Wilson Terrane which constitutes the westernmost tectono-metamorphic belt of the Cambro-Ordovician Ross Orogen at the Pacific end of the Transantarctic Mountains (Fig. 1). The Wilson Terrane is

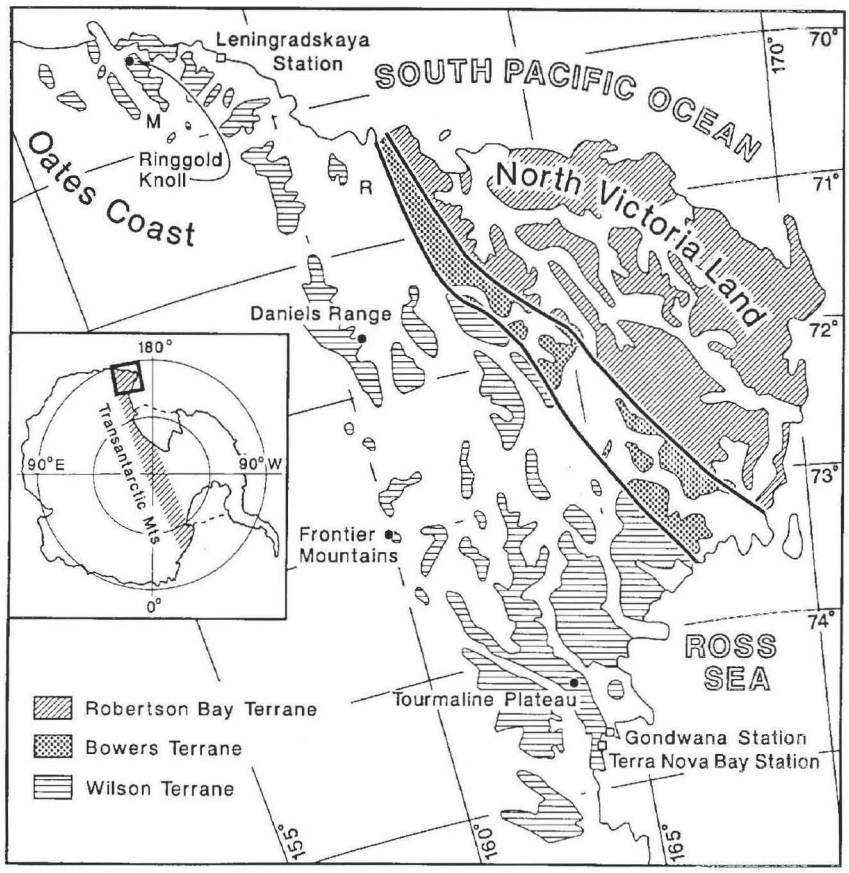

Fig. 1. Geological sketch map of the Oates Coast and North Victoria Land at the Pacific end of the Transantarctic Mountains. Probable Precambrian and Cambro-Ordovician lithologies of the three tectonic terranes are undifferentiated; post-Ordovician lithologies are omitted. Ringgold Knoll denotes the location of the pegmatite investigated, Daniels Range, Frontier Mountains and Tourmaline Plateau the locations of comparable pegmatites within the Wilson Terrane. M, Matusevich Glacier; R, Rennick Glacier.

interpreted as an active continental margin of the Precambrian Antarctic Craton in late Precambrian/early Paleozoic times (e.g. KLEINSCHMIDT and TESSENSOHN, 1987; BORG and DEPAOLO 1991). The rock series within the Wilson Terrane are dominated by amphibolite-facies, mostly migmatitic gneisses, formed during Ross-Orogenic low-pressure metamorphism. Intercalations of granulite-facies rocks are of uncertain age and may represent relics of the Precambrian Antarctic craton (e.g. TALARICO et al., 1987; SCHÜSSLER and TALARICO, 1991; PALMERI et al., 1991; CASTELLI et al., 1991). The metamorphic series were intruded by syn- to post-tectonic igneous rocks of the Granite Harbour suite (GUNN and WARREN, 1962), consisting of minor calc-alkaline to alkaline gabbroic to dioritic intrusives (SCHÜSSLER et al., 1993) and abundant calc-alkaline granitic plutons, both typical of an active continental-margin setting (BORG et al., 1987; VETTER and TESSENSOHN, 1987;

ARMIENTI et al., 1990a, b; BORG and DEPAOLO, 1991). The magmatic activity run out with emplacement of leucocratic aplites and pegmatites and/or fine-grained dykes. Pegmatites occurring in the large-scale Wilson and Exiles thrust systems within the Wilson Terrane (cf. FLÖTTMANN et al., 1993) show extensive high-temperature deformation. This suggests that final cooling of the pegmatites and the wall rocks was due to exhumation of the crystalline basement along these opposingly directed fore-arc and back-arc thrust systems (FLÖTTMANN and KLEINSCHMIDT, 1991, 1993).

Rb-Sr whole-rock dating of Granite Harbour Intrusives (KREUZER et al., 1987; ARMIENTI et al., 1990a, b) resulted mostly in errorchrons because of excess scatter of the data points around a best-fit line, probably reflecting primary isotope inhomogeneities in the magmas (c.f. ADAMS, 1986; BORG et al., 1987). Therefore, the geological meaning of the Rb-Sr whole-rock data which range from about 610 Ma and 470 Ma is questionable (see KREUZER et al., 1987 for details). K-Ar dating of amphiboles, biotites and muscovites from syn- to post-tectonic intrusives of different areas of North Victoria Land however, yielded a restricted age range from about 500 to 480 Ma (KREUZER et al., 1987). Whereas mineral ages of comagmatic biotites and muscovites are mostly concordant, K-Ar dates of amphiboles are about 10 Ma higher than those of comagmatic biotites. Considering the differences in blocking temperature between amphiboles on the one hand and micas on the other hand this suggests a prolonged cooling period of the igneous complexes over the temperature interval between 600 and 300 °C. K-Ar mineral dates slightly younger than 480 Ma may be due to local influxes of heat derived from late-stage magmatic activites. Alternatively, these dates may indicate regional differences in cooling and uplift of basement rocks of the Wilson Terrane.

Analytical methods

Sample preparation and mineral separation were performed by standard methods. Minerals for isotopic and ICP-AES analyses were separated using Wilfley table, magnetic separation and heavy liquid techniques. After repeated washing in an ultrasonic bath in order to remove any surface contaminations, the mineral concentrates were finally hand picked under a binocular microscope to ensure >99% purity.

Mineral compositions were determined in polished thin sections or in polished mounts of separated single grains using a CAMECA SX50 electron microprobe with wavelength-dispersive spectrometers at the University of Würzburg. Operating conditions were 15 kV accelerating voltage, 10 nA sample current measured on the Faraday cage, and 1–2 µm beam size; element peaks and backgrounds were each measured over 20 s, except for Fe (30 s). Synthetic silicate and oxide minerals were used for reference standards. Matrix correction was calculated by the PAP program supplied by CAMECA. An analytical error of less than 1% relative for major elements is verified by repeated measurements on respective standards. For low concentrations, much higher errors must be taken into account. The detection limit is about 0.1 wt.-% for the operating conditions used.

Isotopic analysis of mineral separates and whole-rock powder was carried out at the Federal Institute for Geosciences and Natural Resources (BGR), Hannover. Rb, Sr, Sm, Nd and Ar isotopic analyses were performed using standard isotope-dilution mass-spectrometric techniques (c.f. HARRE et al., 1968; LANGER et al., in press; SEIDEL et al., 1982). Sr, Sm, Nd were measured on a MAT 261, Rb on a VG MM30 and Ar on a MAT CH 4 mass spectrometer. K was determined by flame photometry. $^{40}Ar/^{39}Ar$ dating of muscovite was carried out by incremental step heating analysis on a VG MM1200 mass spectrometer on separates which had been previously irradiated in the scientific nuclear-reactor FRG II, Forschungszentrum GKSS, Geesthacht, using a procedure similar to that

described by BRÖCKER et al. (1993). For calibration of the neutron flux, a well-known intralaboratory muscovite standard (307.7 ± 1.5 Ma) was used as an irradiation monitor. All dates, including those cited, were calculated using the IUGS-recommended constants (STEIGER and JÄGER, 1977). All errors quoted were estimated at a 95% (2-sigma) confidence level.

REE analysis was performed by ICP-AES at the Institute for Mineralogy and Petrography, University of Köln. Mineral dissolution and REE separation were carried out by standard techniques. REE concentrations were determined using Tm as an internal standard and calibrated against REE working curves obtained from analysis of synthetic reference materials. Measured Sm values were corrected for interferences of Nd and Gd. The 2-sigma errors given in Table 4 correspond to twice the standard deviation of three independent measurements.

Petrography

Macroscopically, the pegmatite from Ringgold Knoll mainly consists of quartz and feldspar. Centimetres-wide patches of dark-coloured tourmaline intimately intergrown with quartz in a graphophyric texture are irregularly distributed within the leucocrate matrix (Fig. 2) and are interpreted as late-stage crystallization products. Large red garnets several millimetres in grain-size are enriched next to the tourmaline-rich patches. Green

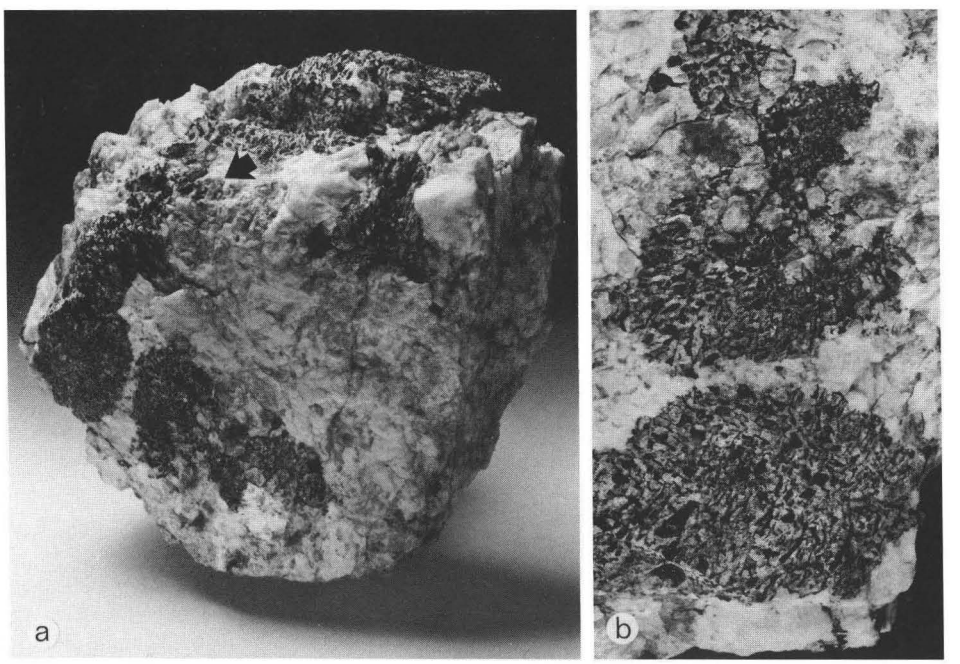

Fig. 2 Characteristic appearance of the Ringgold Knoll pegmatite with quartzofeldspatic matrix and dark patches of late-stage graphophyric intergrowths of tourmaline and quartz. (a): Hand specimen, about 20 cm in diameter; the arrow indicates garnet around dark patches. (b): Detail from (a) with graphophyric textures.

apatite forms aggregates in both, the matrix and the patches. White mica is subordinate but may be locally enriched. Small amounts of blue tourmaline were found at one edge of one rock specimen.

In thin sections the leucocrate matrix is dominated by **K-feldspar** which occurs in large anhedral grains with broad perthitic exsolution lamellae; these lamellae were particularly altered. **Plagioclase** forms euhedral, platy, twinned crystals which have commonly undergone sericitisation. Twinning is sometimes clearly curved, indicating a late tectonic overprint. Anhedral **quartz** shows intensive oscillatory extinction and subgrain formation. **Dark tourmaline** of the tourmaline-quartz patches is usually anhedral and shows discont-inuous optical zonation which only vaguely reflects a core-rim relation. The pleocroitic colour of the cores is pale blue-green to pale green changing to pale olive, light olive, dusky yellow and light-olive brown towards the rims. The outermost rims of some tourmalines are moderate yellow. **Garnet** forms euhedral, sometimes atoll-shaped grains. Except for some larger grains of quartz and rare chloritised biotite, the garnets may show inclusions of accessory **apatite**, **monazite** and **zircon**. These accessories are also found irregularely distributed in the quartz-feldspar matrix. **Dumortierite** and **blue tourmaline** were only detected in heavy-mineral concentrates.

Mineral Chemistry

Major and Minor Elements

Garnet: From microprobe analyses, garnets are solid solutions of almandine (68 mol% core to 70 mol% rim), spessartine (15 mol% core to 18 mol% rim) and pyrope (15 mol% core to 10 mol% rim), with subordinate andradite of about 2 mol% and grossular less than 1 mol%. Four profiles across euhedral grains indicate a slight zonation with an increase of almandine and spessartine components from core to rim at the expense of the pyrope component (Fig. 3 and Table 1).

OLESCH and SCHUBERT (1989) investigated garnet-tourmaline pegmatites from Frontier Mountains which occur in a similar geological position within the Wilson Terrane about 450 km SE of Ringgold Knoll (Fig. 1). Garnets from the Frontier Mountains

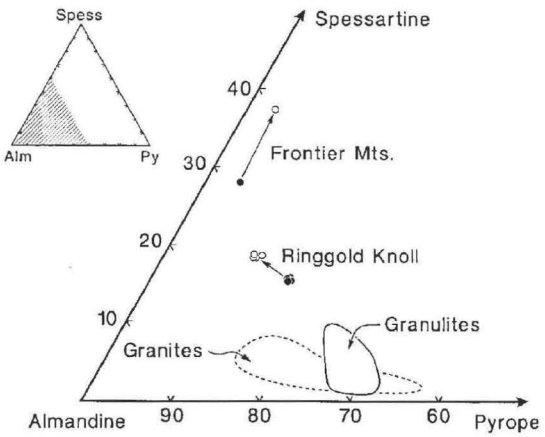

Fig. 3. Garnet compositions from Ringgold Knoll pegmatite compared with those from Frontier Mountains pegmatites (OLESCH and SCHUBERT, 1989), Granite Harbour granites (FENN, 1993) and Oates Coast granulites (SCHÜSSLER, in prep.). Filled circles, core compositions; open circles, rim compositions.

Table 1. Corresponding core and rim compositions of garnets.

	core	rim	core	rim	core	rim	core	rim
wt.-%								
SiO_2	37.19	36.82	36.81	36.57	37.19	36.82	36.87	36.37
TiO_2	0.00	0.05	0.04	0.00	0.01	0.00	0.05	0.01
Al_2O_3	21.12	20.84	20.71	21.00	20.78	20.93	20.92	21.11
Cr_2O_3	0.01	0.00	0.02	0.01	0.03	0.01	0.05	0.00
Fe_2O_3*	0.49	0.15	0.98	0.41	0.86	0.73	0.83	0.32
MgO	3.56	2.58	3.62	2.69	3.84	2.51	3.77	2.82
Cao	0.83	0.73	0.76	0.81	0.86	0.88	0.85	0.78
MnO	6.46	7.44	6.76	7.62	6.64	7.70	6.57	7.33
FeO	30.80	31.06	30.13	30.58	30.03	31.04	30.08	30.57
Total	100.45	99.66	99.83	99.68	100.24	100.62	99.98	99.30
Cations (O = 24)								
Si	5.962	5.986	5.946	5.945	5.970	5.945	5.937	5.928
Al	0.038	0.014	0.054	0.055	0.030	0.055	0.063	0.072
Total	6.000	6.000	6.000	6.000	6.000	6.000	6.000	6.000
Ti	0.000	0.006	0.005	0.000	0.001	0.000	0.006	0.001
Al	3.953	3.980	3.890	3.968	3.901	3.928	3.907	3.984
Cr	0.001	0.000	0.002	0.001	0.004	0.001	0.006	0.000
Fe^{3+}	0.059	0.018	0.119	0.050	0.104	0.089	0.100	0.039
Total	4.013	4.003	4.016	4.018	4.010	4.018	4.019	4.023
Mg	0.851	0.626	0.872	0.652	0.919	0.604	0.906	0.686
Ca	0.143	0.126	0.132	0.141	0.147	0.152	0.146	0.136
Mn	0.877	1.025	0.925	1.049	0.903	1.053	0.896	1.012
Fe^{2+}	4.129	4.223	4.071	4.158	4.031	4.191	4.051	4.167
Total	6.000	6.000	6.000	6.000	6.000	6.000	6.000	6.000
Total	16.013	16.003	16.016	16.018	16.010	16.018	16.019	16.023
Andradite	1.5	0.6	2.2	1.2	2.3	2.2	2.3	1.0
Grossular	0.9	1.5	0.0	1.1	0.0	0.3	0.0	1.3
Almandine	68.8	70.4	67.9	69.3	67.2	69.9	67.5	69.4
Spessartine	14.6	17.1	15.4	17.5	15.1	17.5	14.9	16.9
Pyrope	14.2	10.4	14.5	10.9	15.3	10.1	15.1	11.4

* Fe_2O_3 calculated approaching an ideal site-occupancy of 6, 4, 6

pegmatites have core compositions of 67 mol% almandine, 27 mol% spessartine, 4 mol% Pyrope and 2 mol% grossular. They are clearly zoned with an increase of spessartine component towards the rims mainly at the expense of the almandine component. This inverse zonation, compared with common magmatic garnets, was attributed to the increasing influence of the wall rock and its fluid during garnet formation.

Garnets of Granite Harbour granitic rocks from Oates Coast are generally composed of 60 to 80 mol% almandine, 17 to 37 mol% pyrope and less than 10 mol% spessartine (FENN, 1993). One group of large garnets is characterised by Mg-rich cores, a strong

Table 2. Selected microprobe analysis of tourmaline.

	dark graphophyric tourmaline						blue accessory tourmaline		
	outermost rim moderate yellow		rim light olive	core pale green	core pale blue-green		high Al/Fe		lower Al/Fe
wt.-%									
SiO_2	35.92	35.86	35.27	36.45	35.58	35.33	31.84	31.82	32.63
TiO_2	1.24	1.07	0.55	0.26	0.18	0.01	0.00	0.01	0.00
B_2O_3*	10.71	10.66	10.53	10.70	10.60	10.57	10.93	10.94	10.42
Al_2O_3	33.52	33.52	34.37	35.40	35.34	35.54	48.66	48.89	40.23
Cr_2O_3	0.00	0.00	0.00	0.00	0.03	0.00	0.00	0.05	0.00
MgO	5.49	4.94	3.36	2.86	3.04	2.95	0.05	0.06	0.43
CaO	0.59	0.63	0.67	0.32	0.41	0.50	0.60	0.57	0.15
MnO	0.10	0.08	0.11	0.15	0.11	0.10	0.64	0.50	0.57
FeO**	8.46	9.13	10.38	10.30	10.60	10.51	1.92	1.89	9.45
N_2O	2.05	1.93	1.81	1.63	1.60	1.65	1.47	1.42	1.38
K_2O	0.03	0.02	0.08	0.02	0.02	0.04	0.03	0.01	0.03
Total	98.10	97.82	97.13	98.09	97.49	97.19	96.13	96.16	95.29
Cations (O = 29)									
Si	5.830	5.849	5.822	5.921	5.834	5.812	5.065	5.055	5.441
Al	0.170	0.151	0.178	0.079	0.166	0.188	0.935	0.945	0.559
Total	6.000	6.000	6.000	6.000	6.000	6.000	6.000	6.000	6.000
B	3.000	3.000	3.000	3.000	3.000	3.000	3.000	3.000	3.000
Al	6.000	6.000	6.000	6.000	6.000	6.000	6.000	6.000	6.000
Al	0.243	0.294	0.508	0.698	0.663	0.702	2.188	2.208	1.348
Ti	0.152	0.131	0.068	0.032	0.022	0.001	0.000	0.001	0.000
Cr	0.000	0.000	0.000	0.000	0.003	0.000	0.000	0.006	0.000
Fe	1.148	1.246	1.432	1.400	1.453	1.447	0.256	0.251	1.318
Mn	0.014	0.010	0.015	0.021	0.015	0.014	0.087	0.067	0.080
Mg	1.328	1.200	0.827	0.692	0.742	0.722	0.011	0.015	0.107
Total	2.884	2.881	2.851	2.843	2.899	2.887	2.542	2.549	2.853
Ca	0.103	0.109	0.118	0.056	0.072	0.088	0.102	0.097	0.026
Na	0.644	0.609	0.579	0.514	0.509	0.525	0.455	0.436	0.447
K	0.005	0.004	0.016	0.003	0.005	0.008	0.006	0.003	0.007
Total	0.752	0.722	0.713	0.573	0.586	0.622	0.562	0.536	0.480
Total	18.636	18.604	18.564	18.417	18.485	18.508	18.104	18.084	18.332

* B_2O_3 was calculated assuming 3 cations of B; ** Total iron calculated as FeO

decrease of Mg and increase of Fe and Mn towards the rims, and a texture dominated by decompressional cracks. These garnets were interpreted by FENN (1993) as relic phases from lower crustal granulites, incorporated by granitic magmas during melting processes. This is corroborated by comparable almandine-pyrope contents of garnets from granulitic rocks of the Oates Coast (SCHÜSSLER, in prep.; see Fig. 3).

Garnets from Ringold Knoll pegmatite are intermediate in composition between garnets from Granite Harbour granitic rocks and those from the Frontier Mountains pegmatites (Fig. 3). Because of the minor chemical zonation, euhedral shape and the absence of tectonic fabrics, the garnets are not regarded as a relic phase of the wall rocks or the source rocks of the pegmatite, but have crystallized from the pegmatitic melt.

Tourmaline: From microprobe analyses, the formula was calculated H_2O-free on 29 oxygens with B_2O_3-contents estimated for 3 B cations which is realistic for the tourmaline structure (e.g. HENRY and GUIDOTTI, 1985). Totals of the analyses allow for 2 to 4 wt.-% additional H_2O and Li (see Table 2).

Dark tourmalines from graphophyric tourmaline-quartz patches yield a schorl-dominated composition (X_{Fe} = 0.63–0.67) with significant elbaite and dravite, but only minor liddicoatite components. When using the Al-Fe-Mg or Ca-Fe-Mg diagram of HENRY and GUIDOTTI (1985; see Figs. 4a, b), all analyses from zoned tourmalines plot into a limited field, regardless of their pleocroitic colours. The only exceptions are the moderate yellow outermost rims of some grains which show higher dravite contents (X_{Fe} = 0.48–0.54).

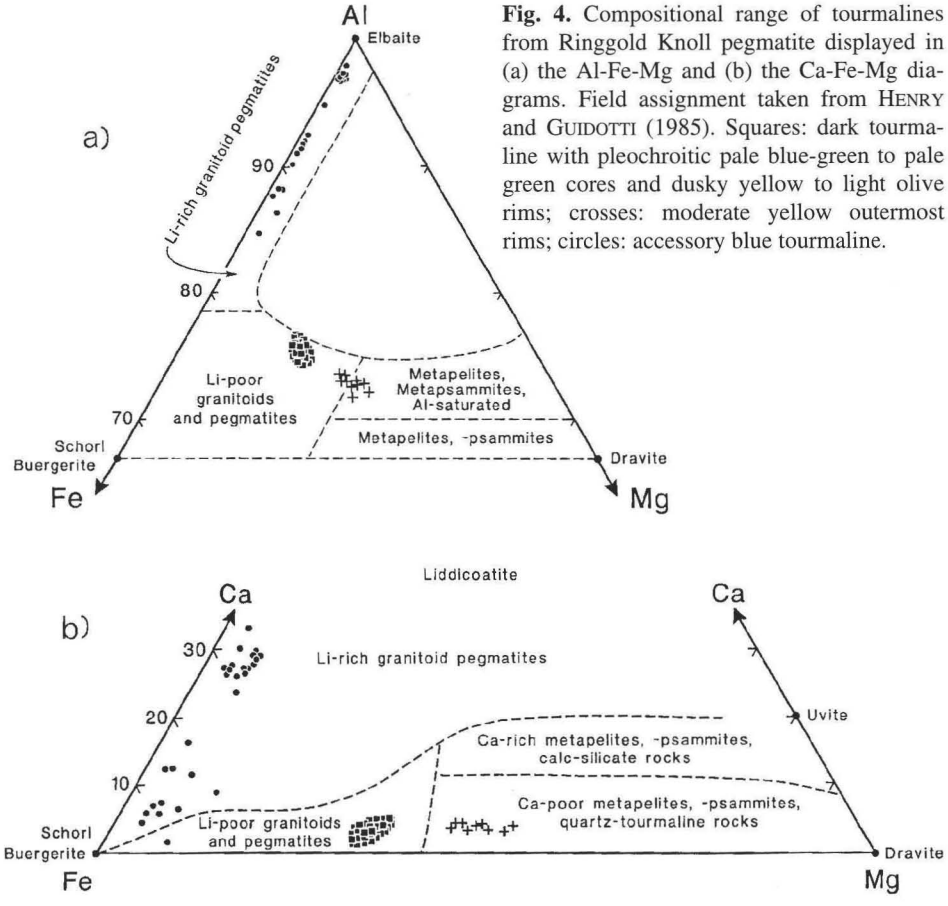

Fig. 4. Compositional range of tourmalines from Ringgold Knoll pegmatite displayed in (a) the Al-Fe-Mg and (b) the Ca-Fe-Mg diagrams. Field assignment taken from HENRY and GUIDOTTI (1985). Squares: dark tourmaline with pleochroitic pale blue-green to pale green cores and dusky yellow to light olive rims; crosses: moderate yellow outermost rims; circles: accessory blue tourmaline.

Looking at the complete chemical analyses (Table 2), a more complicated solid solution for the tourmalines becomes obvious. The deficiency of Na and surplus of Mg and Al in the analyses do not allow for a simple schorl-dravite-elbaite-liddicoatite solid solution. For charge balance of excess Mg and Al without using additional Na, various amounts of uvite and alkali-defect endmembers have to be taken into account.

The optical zonation of dark tourmaline is caused by different TiO_2 contents which vary from 1.0 to 1.2 wt.-% in the moderate yellow outermost rims to 0.5 to 0.6 wt.-% in olive-coloured rims and 0.1 to 0.3 wt.-% in pale-green cores and drop below the detection limit in pale blue-green cores (see Table 2). A similar optical zonation due to different Ti contents was observed by BLACK (1971) in tourmalines of a tourmalinized rhyolite.

A core to rim zonation with an increase of the dravite component at the expense of elbaite and schorl contents, observed between the pale-green, pale blue-green and olive parts on the one hand and the moderate yellow outermost rims on the other hand (Figs. 4a, b), can be regarded as normal zonation. It is typical for tourmalines from leucocratic intrusives and high-grade metamorphic rocks and may be caused by decreasing temperatures during crystallization or by differentiation of the liquid and fluid phases (OLESCH and SCHUBERT, 1987, 1989).

Tourmalines from the Ringgold Knoll pegmatite are similar to those from Frontier Mountains pegmatites concerning composition and normal zonation, but clearly differ from tourmalines of the Tourmaline Plateau pegmatites (Deep Freeze Range, Wilson Terrane, see Fig. 1) which are inversely zoned. Following OLESCH and SCHUBERT (1989), the reason for an inverse zonation is partial assimilation of the metapelitic wall-rock. Pegmatites from Frontier Mountains intruded a granitoid batholith and thus were not influenced in this way. Although the Ringgold Knoll pegmatite penetrated metapelitic to metapsammitic rocks, chemical interaction between wall rock and melt is not expressed by tourmaline compositions or zonations. Most probably, the numerous compact, dry, hardly meltable calc-silicate layers intercalated with the metaclastic wall rock did not permit extensive assimilation or fluid interaction.

The presence of **blue tourmaline** and its identity were confirmed by X-ray powder-diffraction analysis of two grain fractions. Repeated microprobe analysis carried out on these fractions before powdering gave exotic compositions for tourmaline (see Table 2), with unusually low SiO_2 contents of about 30.5 to 32.5 wt.-% and remarkably high Al_2O_3 contents of 48.0 to 49.5 wt.-%. FeO contents usually scatter between 1 and 2 wt.-%, but may increase up to 9.5 wt.-%, apparently substituting for Al_2O_3 (see Table 2). CaO and MnO vary between 0.1 and 1.0 wt.-%. Na_2O contents between 1.5 and 2.0 wt.-% are low if compared with common elbaites (DEER et al., 1986).

Considering the X and Y sites of the mineral formula, the tourmaline could be described as elbaite with subordinate Ca endmember liddicoatite and endmembers which contain Fe and Mn. Because of the deficiency in the X site, Fe and Mn should together with Al rather occupy the Y site of an alkali-defect endmember than form schorl and tsiliasite components. The Y site deficiency is explained by additional Li present in the elbaite and liddicoatite components. The Y site can be filled if the mineral contains about 1 wt.-% Li_2O.

Severe problems arise from the tetrahedral position which is occupied by 6 Si atoms forming Si_6O_{18} rings in common tourmalines (DEER et al., 1986). Microprobe analysis of the blue tourmaline indicate a substitution of about one Si atom by an Al atom to form

rings with an $AlSi_5O_{18}$ composition. Following previous investigations on tourmalines however, the substitution of Si by Al is rather limited (e.g. DEER et al., 1986). FOIT and ROSENBERG (1979) investigated V-bearing tourmaline with $Si_{5.63}Al_{0.37}$ and mentioned that Si-Al substitution in such tourmalines is greater than in other tourmalines. Chemical analysis cited by DEER et al. (1986) indicate a maximal substitution of $Si_{5.66}Al_{0.34}$ for an elbaite from Mozambique. Any analytical problem in our study can be ruled out; a common elbaite from Afghanistan was measured as a control together with the blue Ringgold Knoll tourmaline, and gave correct elbaite compositions. Further investigations are in progress in order to gain more insight into the crystal chemistry of the blue tourmaline from Ringgold Knoll.

Apatite: Two types of apatite, a dominant light green and a subordinate light yellow variety have been recognized in the heavy mineral fractions and investigated by microprobe analysis. P was recorded using the P-Kα line on TAP crystal. The interference of this line with the Ca-Kβ 2nd. order line becomes negligible when using an apatite standard with adequate Ca-content for calibration of P.

Both apatites are hydroxyapatites with Cl-contents of 0.3 to 0.7 wt.-% in the yellow and around 0.1 wt.-% in the green variety. Semiquantitative analysis gave F contents around the detection limit. MnO contents are remarkably high and range between 2.5 and 3.3 wt.-% for green and between 2.3 and 2.9 wt.-% for yellow apatites. Mn enters the apa-

Table 3. Selected microprobe analysis of dumortierite and apatite.

dumortierite					apatite				
wt.-%					wt.-%				
SiO_2	30.94	30.32	30.41	30.49	P_2O_5	42.76	42.65	42.46	42.74
TiO_2	0.12	0.00	0.38	0.33	SiO_2	0.02	0.00	0.00	0.00
B_2O_3*	6.00	5.99	5.96	5.95	CaO	53.06	53.71	53.75	52.59
Al_2O_3	60.90	61.88	60.58	60.35	MnO	3.24	2.70	2.18	2.91
MgO	0.46	0.22	0.55	0.60	FeO**	0.53	0.46	0.73	1.33
FeO**	0.41	0.29	0.38	0.32	Cl	0.07	0.09	0.20	0.48
Total	98.83	98.70	98.26	98.04	Total	99.69	99.61	99.49	100.05
Cations (O = 18)					Cations (O = 25)				
Si	2.990	2.932	2.958	2.971	P	6.010	5.998	5.995	6.016
Al	0.010	0.068	0.042	0.029					
Total	3.000	3.000	3.000	3.000	Ca	9.438	9.559	9.604	9.368
					Mn	0.455	0.380	0.307	0.409
B	1.000	1.000	1.000	1.000	Fe	0.073	0.063	0.101	0.184
					Total	9.967	10.003	10.013	9.961
Ti	0.009	0.000	0.028	0.024					
Al	6.926	6.986	6.903	6.902	Total	15.981	16.002	16.008	15.977
Mg	0.066	0.032	0.080	0.087					
Fe	0.033	0.023	0.031	0.026					
Total	7.034	7.041	7.042	7.039					
Total	11.034	11.041	11.042	11.039					

* B_2O_3 was calculated assuming 1 cation of B; ** Total iron calculated as FeO

tite structure either as Mn^{2+} or Mn^{3+}, thereby replacing Ca, or as Mn^{7+} with a coupled substitution of PO_4^{3-} by MnO_4^{1-} and OH^- by O^{2-}, according to charge balance (VASILIEVA, 1958, cit. in DEER et al., 1962). As in apatites from the Ringgold Knoll pegmatite the XO_4 groups are completely filled with P, Mn should enter the Ca-position. The same probably holds true for Fe; FeO contents vary between 0.5 and 0.8 wt.-% for green and between 1.1 and 1.4 wt.-% for yellow apatites (Table 3).

Dumortierite: Blue dumortierite was found in heavy mineral fractions and its identity confirmed by microprobe and X-ray powder-diffraction analyses. A general formula $(Al,Fe)_7BSi_3O_{18}$ was established by CLARINGBULL and HEY (1958). Besides Fe however, Al may also be substituted by minor amounts of Mg, Ti and vacant positions. Commonly, FeO, MgO and TiO_2 contents are less than 1 wt.-%. Fe_2O_3-contents of up to 3.7 wt.-% were recognized in a dumortierite by BLACK (1973), and TiO_2-contents between 1.0 and 3.1 wt.-% were reported by ALEXANDER et al. (1986), BEUKES et al. (1987) and VRANA (1979). Vacancies were proved by MOORE and ARAKI (1978). The various investigations show that the three-coordinated site of dumortierite is completely filled with B which is not substituted by other elements. The tetrahedral site is also fully filled; a slight Si deficiency is supplemented by Al (ALEXANDER et al., 1986). SCHREYER et al. (1976) describe small amounts of P substituting for Si. The existence of (OH) dumortierite is mentioned by serveral authors. About 0.6 wt.-% H_2O were estimated by ALEXANDER et al. (1986), whereas BEUKES et al. (1987) suggested about 1.6 wt.-% structural H_2O. An approximate average formula for Fe- and Ti-poor dumortierites is given by ALEXANDER et al. (1986):

$$Al_{6.74}(Ti,Fe,Mg,Ca)_{0.14}(Si_{2.92}Al_{0.08})BO_{17.60}(OH)_{0.40}$$

The pegmatite from Ringgold Knoll contains almost pure Al-dumortierite (see Table 3) with Al between 6.90 and 6.99 p.f.u. in the octahedral position. These sites are filled by Mg and subordinate Fe and Ti. The tetrahedral position is occupied by Si ranging between 2.90 and 3.01 cations p.f.u. B_2O_3 was calculated assuming 1 cation p.f.u. The average total of all analyses is 98.55 and indicates H_2O-contents of about 1.0 to 1.5 wt.-%.

Rare Earth Elements (REE)

REE analysis have been carried out on monazite, zircon, apatite, garnet and dark-coloured tourmaline. REE contents and chondrite-normalized REE patterns are given in Table 4 and Fig. 5, respectively.

For **monazite** total REE content is 38.3 wt.-%. Its chondrite-normalized pattern shows a typical enrichment of the light REE and a pronounced negative Eu anomaly. Σ = La + Ce + Pr (MURATA et al., 1957, with presumed 5% of total REE for Pr) is 71 which is close to the average of 70 for monazites from 104 granitic pegmatites. Averages for monazites from granites and alkaline rocks are 76 and 87 respectively (FLEISCHER and ALTSCHULER, 1969).

Zircon contains about 5900 ppm total REE which together with P should form a xenotime component within the zircon lattice by the coupled substitution $REE^{3+} + P^{5+} = Zr^{4+} + Si^{4+}$ (SPEER, 1982). Since highly-charged and smaller-sized cations will preferently substitute for Zr^{4+}, zircons are expected to show patterns enriched in the heavy REE but depleted in light REE (e.g. NAGASAWA, 1970). Zircon from the Ringgold Knoll pegmatite

Table 4. Rare earth element contents of minerals.

ppm	monazite	± 2 σ	zircon	± 2 σ	apatite	± 2 σ	garnet	± 2σ	tour-maline	± 2 σ
La	83 000	2300	384	12	242	2	<0.8	–	2.04	0.12
Ce	180 600	5300	1280	40	740	7	<24	–	4.08	0.19
Nd	78 500	2100	410	11	390	6	<25	–	0.90	0.24
Sm	16 980	460	101	7	161	7	<53	–	0.27	0.27
Eu	214	6	0.73	0,03	4.4	0.4	<1.0	–	0.032	0.008
Gd	12 730	420	124	8	207	15	<14	–	–	–
Dy	7 520	200	504	10	360	5	73.40	1.2	0.085	0.016
Ho	920	40	146	3	59	3	28.40	0.8	–	–
Er	1 350	65	720	15	164	3	160	4	–	–
Yb	760	20	1850	50	169	2	397	8	0.088	0.006
Lu	74	4	364	10	17.8	0.2	75	1.7	0.024	0.007

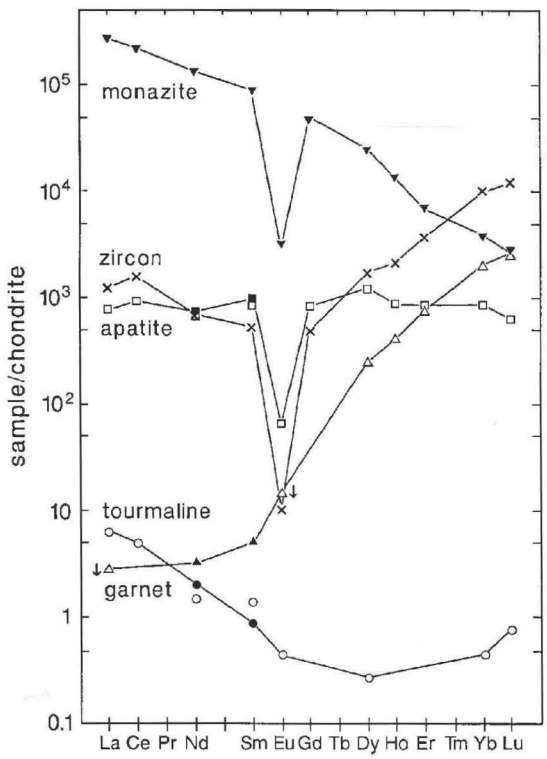

Fig. 5. Chondrite-normalized rare earth element patterns of minerals from Ringgold Knoll pegmatite as determined by ICP-AES analysis. Filled symbols for Sm and Nd of apatite, garnet and tourmaline are isotope-dilution data by mass spectometric analysis (compare Table 6).

is characterized by a strong heavy REE enrichment, but additionally shows elevated concentrations of the light REE (see Fig. 5). Light REE enriched patterns may be due to contamination of the zircon fraction as was shown by NAGASAWA (1970). In our case, the light REE enrichment is probably due to very small amounts of monazite intergrown with zircon.

In **apatite**, 2500 ppm total REE have been determined which could have entered the structure by the substitutions $Na^{+} + REE^{3+} = 2Ca^{2+}$, $REE^{3+} + Si^{4+} = Ca^{2+} + P^{5+}$, or $REE^{3+} + O^{2-} = Ca^{2+} + F^{-}$ (BURT, 1989). Since the light green apatites from Ringgold Knoll contain up to 0.2 wt.-% Na_2O and SiO_2 contents lie below the detection limit, the first alternative appears the most realistic. The REE pattern is more or less flat with a pronounced negative Eu anomaly. REE patterns of apatites from acid rocks are either enriched in the light REE or flat, whereas those of basic or alkaline rocks are generally enriched in light REE (FLEISCHER and ALTSCHULER, 1969). Correspondingly, the Σ = La + Ce + Pr (with presumed 4.6% of total REE for Pr) is 45 and thus close to the average of 47 for apatites from 14 granitic pegmatites; Σ for apatites from granites is 55, from basites 69 and from alkaline rocks 78 (FLEISCHER and ALTSCHULER, 1969).

Garnet shows low REE concentrations of about 750 ppm. According to BURT (1989), $REE^{3+} + Al^{3+} = Ca^{2+} + Si^{4+}$ or $REE^{3+} + Al^{3+} = Mn^{2+} + Si^{4+}$ are the most practical ways of substituting REE into garnet. As garnet is highly selective for heavy REE, garnets from the Ringgold Knoll pegmatite are typically enriched in these elements and give a heavy REE pattern similar to that of zircon (MEAGHER, 1982).

Among the minerals investigated, **tourmaline** yields the lowest REE concentrations of less than 10 ppm. The pattern shows a slight enrichment of the light REE, but also of Yb and Lu. A similar "basin-shaped" pattern and low REE contents for tourmaline are described by ALDERTON et al. (1980). From their results a very limited capacity of tourmaline for the incorporation of REE can be inferred even in REE-rich environment. Thus the low REE concentrations of the Ringgold Knoll tourmalines are probably due to crystal-chemistry restrictions rather than being the result of its late-stage crystallization in a low-REE environment.

Isotopic data

The analytical data are listed in Table 5 for K-Ar and in Table 6 for Rb-Sr and Sm-Nd. The analytical results of the ^{40}Ar-^{39}Ar experiments on two muscovite separates are shown only graphically (Fig. 6); a list of the analytical data is available on request.

K-Ar determination of two muscovite separates yielded concordant dates of 475.1 ± 5.3 and 477.0 ± 5.7 Ma. **^{40}Ar-^{39}Ar** analysis of the muscovites, however, indicate

Table 5. K-Ar analytical data of RK12 muscovite[1]).

sample	K (wt.-%)	rad. Ar (nl/g STP)	rad. Ar (%)	date ± 2 sigma (Ma)
msc 500–250 µm	8.895	187.9	99.3	475.1 ± 5.3
msc 250–125 µm	8.746	185.6	99.0	477.0 ± 5.7

[1]) Argon concentrations in nanoliter at standard conditions (nl/g STP). Ar analytical data are corrected for blank by using the mean values of short period of blank analyses. Mean standard deviation (2 sigma) of radiogenic argon is about 0.3%, of potassium about 0.5%. Our K-Ar date of the standard glaucony Gl-O is 1% younger than the mean value of the compilation of ODIN (1982).

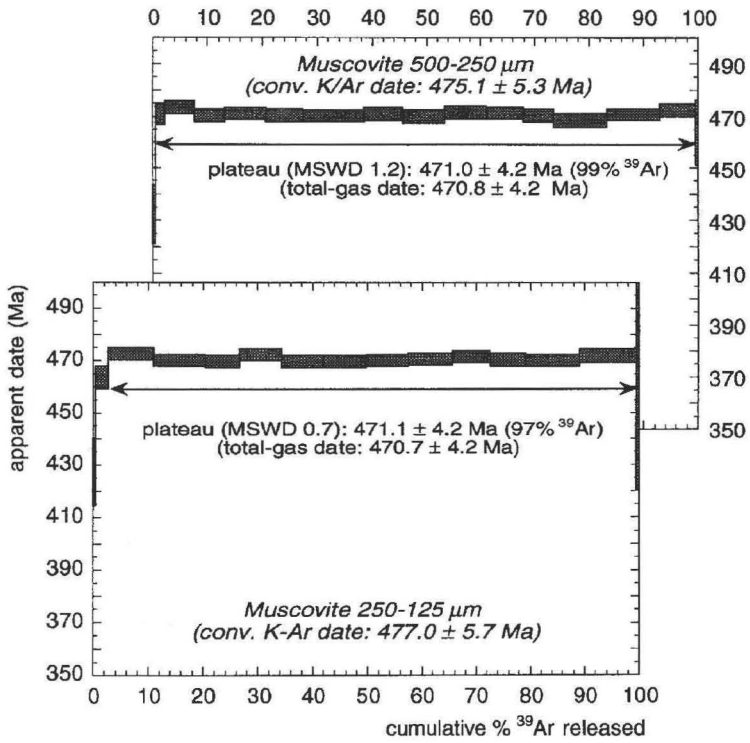

Fig. 6. ^{40}Ar-^{39}Ar spectra of two muscovite separates from Ringgold Knoll pegmatite. Vertical extension of the boxes represent 2-sigma intra-analysis errors.

slightly lower total-gas dates of 470.8 ± 4.2 and 470.7 ± 4.2 Ma (Fig. 6). An explanation for the discrepancy between conventional K-Ar dates and Ar-Ar total-gas dates which is significant on the 1-sigma level cannot be given. Because of the low amount of separated muscovite available, the K-Ar and Ar-Ar data cannot be verified by replicate analysis. For both muscovite separates the incremental step heating experiments yielded plateau ages of 471.0 ± 4.2 Ma over 99% (size fraction 500–250 µm) and of 471.1 ± 4.2 Ma over 97% ^{39}Ar released (size fraction 250–125 µm) which exclude any significant secondary disturbances of the K-Ar system of the igneous muscovite. Furthermore, the 471 ± 4 Ma plateau dates suggest that final cooling of the pegmatite to temperatures below about 350 °C, i.e. the K-Ar blocking temperature of muscovite, occurred during Middle Ordovician times.

Rb-Sr isotopic data for apatite, monazite, garnet, muscovite, tourmaline and whole-rock do not fit a single straight line on the isochron diagram (Fig. 7a–c). Only for monazite, apatite and whole rock a statistically meaningful linear arrangement of more than two data points is obtained. These three data points define an isochron (MSWD = 0.4) which corresponds to an age of 492.0 ± 8.0 Ma; its initial $^{87}Sr/^{86}Sr$ ratio is 0.7315 ± 0.0003. This isochron age is interpreted as the best estimate for the time of igneous crystallization of the pegmatite. With respect to this isochron, the data points of two muscovite separates

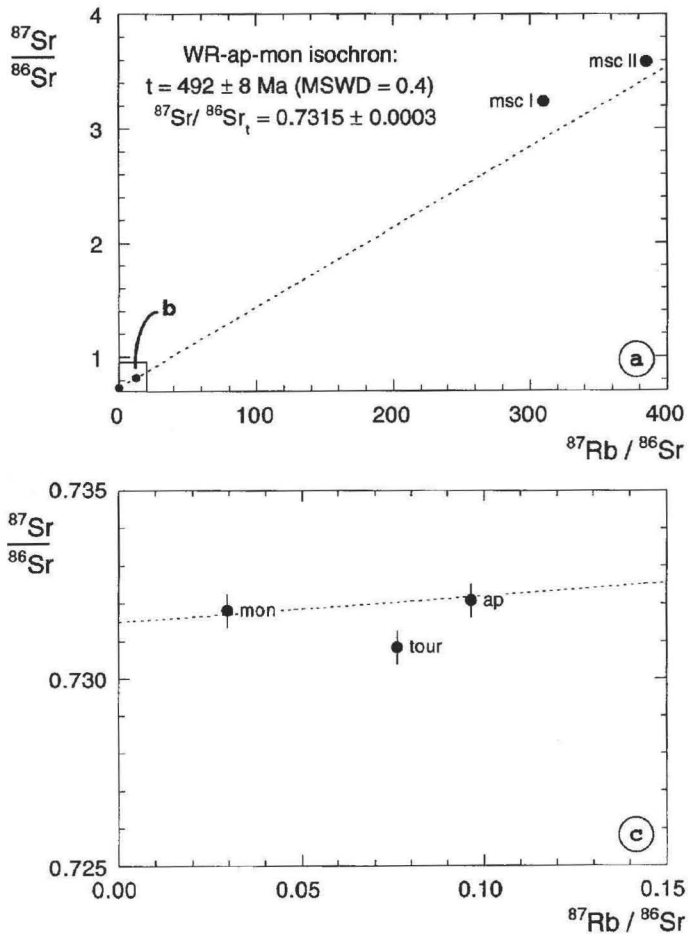

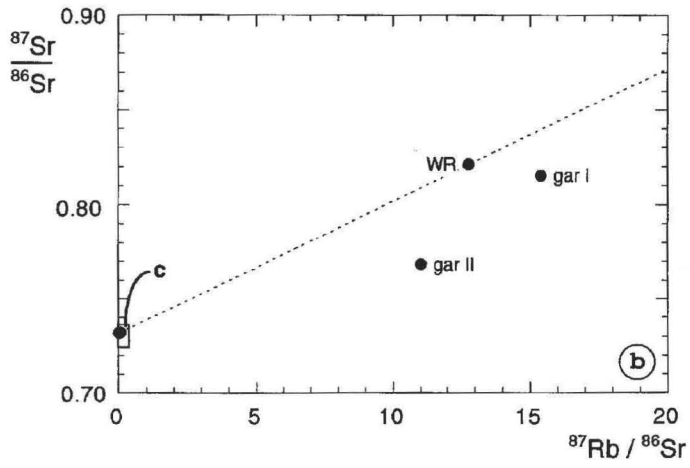

Fig. 7. a–c. Present day Sr isotope compositions of Ringgold Knoll pegmatite whole-rock and minerals versus $^{87}Rb/^{86}Sr$. Due to the very large spread in the isotopic ratios the data of two muscovite fractions are plotted in Fig. 7a, those of whole-rock and two garnet separates in Fig. 7b, and those of apatite, monazite and tourmaline in Fig. 7c. Vertical bars in Fig. 7c indicate 2-sigma errors in $^{87}Sr/^{86}Sr$.

Table 6. Rb-Sr and Sm-Nd analytical data of RK12 whole rock and minerals[1]).

sample[2])	Rb	Sr	$^{87}Rb/^{86}Sr$	$^{87}Sr/^{86}Sr$	Sm	Nd	$^{147}Sm/^{144}Nd$	$^{143}Nd/^{144}Nd$
	ppm				ppm			
WR	141.7	32.45	12.787	0.82116	14.79	62.55	0.1424	0.512009
ap	1.226	36.89	0.0965	0.73209	191.8	444.0	0.2655	0.512404
mon	0.3968	38.95	0.0296	0.73181	1.901%	8.633%	0.1326	0.511982
gar I	0.5431	0.1030	15.419	0.81524	1.008	1.883	0.3222	0.512618
gar II[3])	0.0749	0.0198	11.031	0.7683	–	–	–	–
msc I	578.1	6.729	310.38	3.2391	0.4512	1.653	0.164	–
msc II	591.2	5.685	385.64	3.5861	0.5640	1.978	0.172	–
tour	0.3123	11.896	0.0762	0.73083	0.1832	1.213	0.0910	0.511855

[1]) Average uncertainties (2 sigma) in $^{87}Rb/^{86}Sr$, $^{87}Sr/^{86}Sr$, $^{147}Sm/^{144}Nd$ and $^{143}Nd/^{144}Nd$ are 1.5%, 0.06%, 1.4%, and 0.01%, respectively. $^{87}Sr/^{86}Sr$ ratios are normalized to $^{86}Sr/^{88}Sr = 0.1994$, $^{143}Nd/^{144}Nd$ ratios to $^{146}Nd/^{144}Nd = 0.7219$. In the course of this study the NBS 987 Sr standard yielded $^{87}Sr/^{86}Sr = 0.710262 \pm 5$ (n = 5), the La Jolla Nd standard gave $^{143}Nd/^{144}Nd = 0.511869 \pm 6$ (n = 9).

[2]) Abbreviations: WR whole rock, ap apatite, mon monazite, gar garnet, msc muscovite, tour tourmaline.

[3]) HF and HCl leached mineral separate (compare text for details).

plot above the line (Fig. 7a), while those of garnet (Fig. 7b) and tourmaline (Fig. 7c) plot below the line. All indicate various degrees of post-igneous disturbances of their Rb-Sr isotope compositions. The differences in $^{87}Rb/^{86}Sr$ and $^{87}Sr/^{86}Sr$ between *msc I* (grain-size fraction 250–125 µm alone) and *msc II* (a mixture of 250–125 µm and 500–250 µm fractions) suggest that the Rb-Sr system of the finer-grained muscovites suffered from post-igneous low-temperature processes.

The off-line positions of the garnet (*gar I*; Table 6) and tourmaline data points are not explained by modifications of their Rb-Sr isotopic compositions in the course of geological processes. Instead, they are likely due to surface contaminations and/or to laboratory handling of the samples. Both minerals caused severe problems during sample dissolution. In the course of the repeated attempts to dissolve these minerals, both samples could have suffered from blank contaminations. In case of the garnet which shows very low concentrations of both Rb and Sr, this may have resulted in an increase in Rb and therefore also in $^{87}Rb/^{86}Sr$ but a decrease in $^{87}Sr/^{86}Sr$ due to the relatively low Sr isotopic ratios of the chemical reagents. In order to test the influence of surface contaminations on the Rb-Sr isotopic composition of garnet, a second hand-picked sample was leached in 5% HF and in 2.5 N HCl and afterwards washed with two-bottle distilled acetone in an ultrasonic bath prior to dissolution. Optical examination of the leached separate did not show any evidence of garnet dissolution due to this chemical treatment. Compared to the unleached garnet sample (*gar I*; Table 6) this separate yielded distinctly lower Rb and Sr concentrations and also a lower $^{87}Sr/^{86}Sr$ ratio (*gar II*; Table 6). This suggests that the Rb-Sr data of *gar I* are largely obscured by the presence of surface contamination. Since it is not clear to which extent these surface contaminants have been removed in the course of the leaching procedure, *gar II* may still have been contaminated and its Rb-Sr data can therefore not be used for dating purposes. Moreover, the analytical data of the leached garnet show that this igneous phase is practically free of Rb and Sr and is therefore not a suitable candidate for Rb-Sr dating.

Contrary to garnet, the data point for tourmaline plots very close to the isochron and indicates a lesser degree of contamination. An isochron calculation using the Rb-Sr data of whole-rock, apatite, monazite and tourmaline shifts the age to a very slightly higher value of 494 Ma but drastically increases the MSWD value to about 20. Because of its very low $^{87}Rb/^{86}Sr$ ratio, addition of blank Rb to the tourmaline sample will result in only a small increase in the $^{87}Rb/^{86}Sr$ ratio. In this case, the major contamination is probably due to addition of blank Sr, which results in a small shift of the tourmaline data point to lower $^{87}Sr/^{86}Sr$ ratios.

Sm-Nd isotopic data of all but one of the igneous minerals investigated and the whole rock sample fit a single straight line which, if taken as an isochron (MSWD = 0.9), defines an age of 500 ± 40 Ma and an initial $^{143}Nd/^{144}Nd$ ratio of 0.51155 ± 0.00006 (Fig. 8). Because of the good line fit of all data points blank or surface contaminations of Sm and Nd seem to have been negligible. Due to its very low REE content duplicate Nd analyses of muscovite were unsuccessful. The 2-sigma error in the isochron date (± 40 Ma) does not tightly constrain the age of pegmatite emplacement. On the 1-sigma level, however, the Sm-Nd age is identical with the Rb-Sr isochron date but different from the K-Ar and Ar-Ar ages of igneous muscovite and, therefore, supports the geological interpretation of the Rb-Sr isochron age given above.

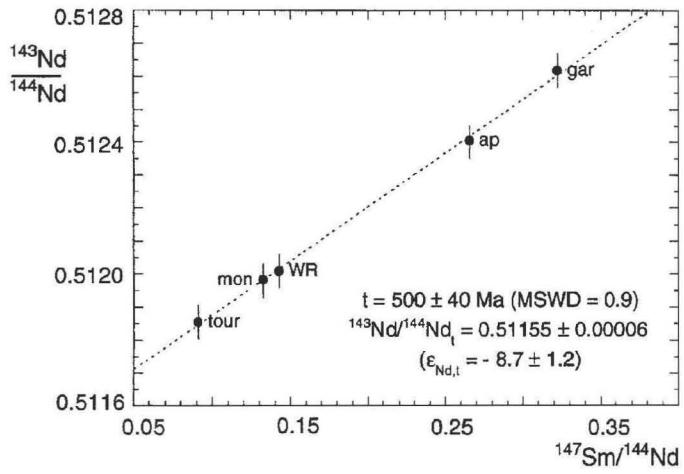

Fig. 8. Present day Nd isotope compositions of Ringgold Knoll pegmatite whole-rock and minerals versus $^{147}Sm/^{144}Nd$. Vertical bars indicate 2-sigma errors in $^{143}Nd/^{144}Nd$.

Conclusions

The mineral association in the Ringgold Knoll pegmatite consists of feldspar, quartz, muscovite, garnet, dark and blue tourmaline, apatite, monazite, zircon and dumortierite. The spacial distribution of these minerals suggests that the igneous crystallization sequence started with the formation of feldspar, quartz and subordinate muscovite making up the leucocratic matrix of the pegmatite. Due to crystallization of minerals rich in Si, Al, K and Na the pegmatitic melt experienced an increase in Fe, Mg and Mn which led initially to the growth of large matrix garnets and finally, combined with a late-stage boron enrichment, to the formation of a tourmaline rich in schorl and dravite components. Texturally, this tourmaline occurs in graphophyric intergrowths with quartz which often are surrounded by the earlier-formed matrix garnets. Furthermore, elevated B and Al contents triggered crystallization of accessory dumortierite and a second, blue tourmaline with an unusual Al-rich composition.

Chemical zonation patterns of dark tourmaline from Ringgold Knoll do not contain evidence of intensive interaction of the pegmatite melt with its wall rocks as was argued for pegmatitic tourmalines from Tourmaline Plateau by Olesch and Schubert (1989). Because of their almandine-spessartine-pyrope composition and missing microfabrics, the garnets are, in contrast to certain garnets from Granite Harbour granites (Fenn, 1993), not relics of the probably granulitic pegmatite source rocks but rather newly crystallized from the melt.

The time of pegmatite emplacement is at present best constrained by Rb-Sr and Sm-Nd isochron ages of 492 ± 8 Ma and 500 ± 40 Ma, respectively. U-Pb dating on igneous monazite and zircon is in progress in order to verify this. An initial $^{87}Sr/^{86}Sr$ ratio of 0.7315 ± 0.0003 and ϵ Nd,t of –8.7 ± 1.2 clearly support an origin of the magma from highly evolved crustal source rocks. In its initial Sr isotopic composition, the Ringgold Knoll pegmatite plots outside the range of values found for Granite Harbour Intrusives from the eastern margins of the Wilson Terrane in North Victoria Land. These are generally more primitive in Sr and also partly in Nd isotopic compositions (cf. Adams, 1986; Borg et al., 1987; Kreuzer et al., 1987). As a result it is unclear whether magma genesis of the Ring-

gold Knoll pegmatite forms part of the subduction-related Granite Harbour igneous activity or is due to late-stage syncollision melting of the crust.

Judging from K-Ar and ^{40}Ar-^{39}Ar ages of about 470 Ma for igneous muscovite, the pegmatite experienced a rather slow cooling to temperatures below about 350 °C. Interestingly, concordant K-Ar muscovite and biotite ages of about 470 to 475 Ma were also reported by KREUZER et al. (1987) for a pegmatite from the Daniels Range located some 250 km southeast of Ringgold Knoll (Fig. 1). Minor high-temperature deformation phenomena observed for the Ringgold Knoll pegmatite indicate tectonic activity during its emplacement or during the prolonged subsolidus history at elevated temperatures. The Ringgold Knoll pegmatite is located just east of the mylonitic Exiles thrust which together with the Wilson thrust forms two major detachment systems of the Wilson Terrane (FLÖTTMANN and KLEINSCHMIDT, 1991). As was argued by these authors, exhumation of the central Wilson Terrane probably occurred by thrusting of its crystalline basement rocks over lower-grade series to the east and west. With respect to this model, the muscovite ages of the Ringgold Knoll pegmatite may give an estimate of the time of final cooling of the high-grade Wilson metamorphics and Granite Harbour Intrusives of the Oates Coast area in the course of exhumation.

Acknowledgements

The authors wish to thank MONIKA BOCKRATH, MARGOT METZ, HORST KLAPPERT, PETER MACAJ and HENRYK SCHYROKI for laboratory work at the BGR and AXEL HÖHNDORF and HEINZ-GÜNTHER STOSCH for stimulating discussion. KLAUS-PETER KELBER is thanked for preparing part of the figures, PETER SPÄTHE for preparation of the thin-sections and NIGEL COOK for a critical review of the text. HEINZ-GÜNTHER STOSCH and an unknown laboratory assistant kindly carried out the REE analysis. Many thanks are due to all who contributed to the success of the fieldwork with their logistic help. Financial support from the Bundesanstalt for Geowissenschaften und Rohstoffe and from the Deutsche Forschungsgemeinschaft is greatfully acknowledged. Special thanks are due to STEFAN ROSE who was a helpful companion during the fieldwork.

References

ADAMS, C. J.: Age and ancestry of the metamorphic rocks of the Daniels Range, USARP Mountains, Antarctica. In: STUMP, E. (ed.): Geological Investigations in Northern Victoria Land. Amer. Geophys. Union, Antarct. Res. Ser. **46** (1986), 25–38.

ALDERTON, D. H. M., PEARCE, J. A. and POTTS, P. J.: Rare earth element mobility during granite alterations; evidence from southwest England. Earth Planet. Sci. Lett. **49** (1980), 149–165.

ALEXANDER, V. D., GRIFFEN, D. T. and MARTIN, T. J.: Crystal chemistry of some Fe- and Ti-poor dumortierites. Amer. Min. **71** (1986), 786–794.

ARMIENTI, P., GHEZZO, C., INNOCENTI, F., MANETTI, P., ROCCHI, S. and TONARINI, S.: Granite Harbour Intrusives from North Victoria Land between David and Campbell Glaciers: new geochronological data. Zbl. Geol. Paläont. **1/2** (1990a), 63–74.

ARMIENTI, P., GHEZZO, C., INNOCENTI, F., MANETTI, P., ROCCHI, S. and TONARINI, S.: Isotope geochemistry and petrology of granitoid suites from Granite Harbour Intrusives of the Wilson Terrane, North Victoria Land, Antarctica. Eur. J. Mineral. **2** (1990b), 103–123.

BEUKES, G. J., SLABBERT, M. J., DEBRUIYN, H., BOTHA, B. J. V., SCHOCH, A. E. and VAN DER WESTHUIZEN, W. A.: Ti-dumortierite from the Keimoes area, Namaqua mobile belt, South Africa. N. Jb. Miner. Abh. **157** (1987), 303–318.

BLACK, P. M.: Tourmalines from Cuvier Island, New Zealand. Mineral. Mag. **38** (1971), 374–376.

BLACK, P. M.: Dumortierite from Karikari Peninsula: a first record in New Zealand. Mineral. Mag. **39** (1973), 245.

BORG, S. G. and DEPAOLO, D. J.: A tectonic model of the Antarctic Gondwana margin with implications for southeastern Australia. Tectonophys. **196** (1991), 339–358.

BORG, S. G., STUMP, E., CHAPPELL, B. W., MCCULLOCH, M. T., WYBORN, D., ARMSTRONG, R. L. and HALLOWAY, J. R.: Granitoids of northern Victoria Land, Antarctica: Implications of chemical and isotopic variations to regional crustal structure and tectonics. Am. J. Sci. **287** (1987), 127–169.

BRÖCKER, M., KREUZER, H., MATTHEWS, A. and OKRUSCH, M.: $^{40}Ar/^{39}Ar$ and oxygen isotope studies of polymetamorphism from Tinos Island, Cycladic blueschist belt, Greece. J. Metamorphic Geol. **11** (1993), 223–240.

BURT, D. M.: Compositional and phase relations among rare earth element minerals. Reviews in Mineral. **21** (1989), 259–307.

CASTELLI, D., LOMBARDO, B., OGGIANO, G., ROSETTI, P. and TALARICO, F.: Granulite Facies Rocks of the Wilson Terrane (northern Victoria Land): Campbell Glacier. Mem. Soc. Geol. It. **46** (1991), 197–203.

CLARINGBULL, G. F. and HEY, M. H.: New data for dumortierite. Mineral. Mag. **31** (1958), 901–907.

DEER, W. A., HOWIE, R. A. and ZUSSMAN, J.: Rock-Forming Minerals: Non-Silicates. Longman, New York (1962).

DEER, W. A., HOWIE, R. A. and ZUSSMAN, J.: Rock-Forming Minerals: Disilicates and Ringsilicates. Longman, New York (1986).

FENN, G.: Petrogenese der Granite Harbour Intrusives in Nord Victoria Land und der Prince Albert Mountains (Antarktis). Unpubl. Dr.-Thesis, Univ. Bremen (1993), 174 p.

FLEISCHER, M. and ALTSCHULER, Z. S.: The relationship of rare-earth composition of minerals to geological environment. Geochim. Cosmochim. Acta **33** (1969), 725–732.

FLÖTTMANN, T. and KLEINSCHMIDT, G.: Opposite thrust systems in northern Victoria Land, Antarctica: Imprints of Gondwana's Paleozoic accretion. Geology **19** (1991), 45–47.

FLÖTTMANN, T. and KLEINSCHMIDT, G.: The Structure of Oates Land and Implications for the Structural Style of Northern Victoria Land, Antarctica. Geol. Jb. **E 47** (1993), 419–436.

FLÖTTMANN, T., GIBSON, G. M. and KLEINSCHMIDT, G.: Structural continuity of the Ross and Dalamerian orogens of Antarctica and Australia along the margin of the paleo-Pacific. Geology **21** (1993), 319–322.

FOIT, F. F. and ROSENBERG, P. E.: The structure of vanadium-bearing tourmaline and its implications regarding tourmaline solid solutions. Amer. Min. **64** (1979), 788–798.

GUNN, B. M. and WARREN, G.: Geology of Victoria Land between the Mawson and Mulock Glaciers, Antactica. Bull. NZ. Geol. Surv. **71** (1962), 1–157.

HARRE, W., KREUZER, H., LENZ, H., MÜLLER, P., WENDT, I. and SCHMIDT, K.: Rb/Sr- and K/Ar-Altersbestimmungen an Gesteinen des Ötztalkristallins. Geol. Jb. **86** (1968), 797–826.

HENRY, D. J. and GUIDOTTI, C. V.: Tourmaline as a petrogenetic indicator mineral: an example from the staurolite-grade metapelites of NW Maine. Amer. Min. **70** (1985), 1–15.

KLEINSCHMIDT, G. and TESSENSOHN, F.: Early Paleozoic westward directed subduction at the Pacific margin of Antarctica. In: MCKENZIE, G. D. (ed.): Gondwana Six: Structure, tectonics and geophysics. Amer. Geophys. Union, Geophys. Monogr. Series **40** (1987), 89–105.

KREUZER, H., HÖHNDORF, A., LENZ, H., MÜLLER, P. and VETTER, U.: Radiometric ages of pre-Mesozoic rocks from Northern Victoria Land, Antarctica. In: MCKENZIE, G. D. (ed.): Gondwana Six: Structure, tectonics and geophysics. Amer. Geophys. Union, Geophys. Monogr. Series **40** (1987), 31–47.

LANGER, C., ALTHERR, R., HENJES-KUNST, F., SATIR M. and OTTO, J.: Genesis of the composite Oberkirch pluton (Schwarzwald, Germany) and its use as a probe for deeper parts of the crust. Contrib. Mineral. Petrol., in press.

MEAGHER, E. P.: Silicate garnets. Reviews in Mineral. **5**, 2nd ed. (1982), 25–66.

MOORE, P. B. and ARAKI, T.: Dumortierite, Si3B(Al6.75_0.25O17.25(OH)0.75): a detailed structure analysis. N. Jb. Mineral. Abh. **132** (1978), 231–241.

MURATA, K. J., ROSE, H. J., CARRON, M. K. and GLASS, J. J.: Systematic variation of rare earths in cerium-earth minerals. Geochim. Cosmochim. Acta **11** (1957), 141–161.

NAGASAWA, H.: Rare earth concentrations in zircons and apatites and their host dacites and granites. Earth Planet. Sci. Lett. **9** (1970), 359–364.

OLESCH, M. and SCHUBERT, W.: Different Zoning Pattern in Tourmalines from North Victoria Land Pegmatites, Antarctica. Polarfoschungen **57** (1987), 9–15.

OLESCH, M. and SCHUBERT, W.: Aplite and Pegmatite Mineralogy of the Granite Harbour Intrusives, North Victoria Land, Antarctica. Geol. Jb. **E 38** (1989), 257–275.

PALMERI, R., TALARICO, F., MECCHERI, M., OGGIANO, G., PERTUSATI, P. C., RASTELLI, N. and RICCI, C. A.: Progressive Deformation and Low Pressure/High Temperature metamorphism in the Deep Freeze Range, Wilson Terrane, northern Victoria Land, Antarctica. Mem. Soc. Geol. It. **46** (1991), 179–195.

SCHREYER, W., ABRAHAM, K. and BEHR, H. J.: Sapphirine and Associated Minerals from the Kornerupine Rock of Waldheim, Saxony. N. Jb. Mineral. Abh. **126** (1976), 1–27.

SCHÜSSLER, U. and TALARICO, F.: Granulite facies rocks from the Ross orogenic belt, North-Victoria-Land, Antarctica. Eur. J. Mineral. **3 Beih. 1** (1991), 241.

SCHÜSSLER, U., SKINNER, D. N. B. and ROLAND, N.: Subduction-related Mafic to Intermediate Plutonism in the Northwestern Wilson Terrane, North Victoria Land, Antarctica. Geol. Jb. **E 47** (1993), 389–418.

SEIDEL, E., KREUZER, H. and HARRE, W.: A late Oligocene/early Miocene high pressure belt in the external Hellenides. Geol. Jb. **E 23** (1982), 165–206.

SPEER, J. A.: Zircon. Reviews in Mineral **5**, 2nd ed. (1982), 67–112.

STEIGER, R. H. and JÄGER, E.: Subcommission on geochronology: the use of decay constants in geo- and cosmochronology. Earth Planet. Sci. Lett. **36** (1977), 359–362.

TALARICO, F., MEMMI, I., LOMBARDO, B. and RICCI, C. A.: Thermo-barometry of granulite rocks from the Deep Freeze Range, North Victoria Land, Antarctica. Mem. Soc. Geol. It. **33** (1987), 131–142.

VETTER, U. and TESSENSOHN, F.: S- and I-type granitoids of North Victoria Land, Antarctica, and their inferred geotectonic setting. Geol. Rundsch. **76** (1987), 233–243.

VRANA, S.: A polymetamorphic assemblage of grandidierite, kornerupine, Ti-rich dumortierite, tourmaline, sillimanite and garnet. N. Jb. Miner. Mh. (1979), 22–33.

Authors' addresses: Dr. F. HENJES-KUNST, Bundesanstalt für Geowissenschaften und Rohstoffe, Postfach 510153, D - 30631 Hannover, Germany; Dr. U. SCHÜSSLER, Mineralogisches Institut, Am Hubland, D - 97074, Germany.